

## The influence of the intermediate principal stress on rock failure behaviour: A numerical study

Peng-Zhi Pan <sup>a,\*</sup>, Xia-Ting Feng <sup>a</sup>, J.A. Hudson <sup>b</sup>

<sup>a</sup> State Key Laboratory of Geomechanics and Geotechnical Engineering, Institute of Rock and Soil Mechanics, Chinese Academy of Sciences, Wuhan, 430071, China

<sup>b</sup> Department of Earth Science and Engineering, Imperial College, London SW7 2AZ, UK

### ARTICLE INFO

#### Article history:

Received 7 March 2011

Received in revised form 10 October 2011

Accepted 11 October 2011

Available online 19 October 2011

#### Keywords:

Rock failure process

Intermediate principal stress effect

Polyaxial compression

Elasto-plastic cellular automaton

Heterogeneity

### ABSTRACT

The influence of the intermediate principal stress on rock strength has been studied comprehensively by previous researchers. However, the reason why rock strength firstly increases and subsequently decreases with the increase of intermediate principal stress is still unclear. In this paper, the mechanism of the intermediate principal stress effect on rock failure behaviour is revealed through a numerical method using the EPCA3D system (Elasto-Plastic Cellular Automaton). In this study, both homogeneous and heterogeneous rocks are considered. The heterogeneity of a rock specimen is modelled by introducing Weibull's statistical distribution. Two criteria, i.e. the Drucker-Prager and Mohr-Coulomb models, are used to determine whether a mesoscopic element in the rock specimen is in a failure state or not during the polyaxial stress loading process. The EPCA3D simulation reproduces the typical phenomenon of the intermediate principal stress effect that occurs in some rock experiments. By studying the EPCA3D simulated acoustic emission and complete stress-strain curves illustrating failure initiation, propagation and coalescence in the failure process of rocks, the essence of the intermediate principal stress effect is tracked. It is concluded that the heterogeneous stress distribution induced by the natural heterogeneity of rocks and the effect of the loading platen are two of the reasons producing the intermediate stress effect. Studies indicate that a moderate intermediate principal stress delays the onset of local failure, which in turn leads to an increase in the rock strength. However, once the intermediate principal stress reaches a certain value, local failure will be formed through the application of the intermediate principal stress. It is the number of failed elements in the pre-peak region that determines whether the rock strength decreases or not. The extent of rock strength reduction when the intermediate principal stress reaches a certain value is lessened with the increase in the minimum principal stress.

© 2011 Elsevier B.V. All rights reserved.

### 1. Introduction

The study of rock failure processes under complex stress conditions is an important subject in rock mechanics. Moreover, with geotechnical engineering extending to greater depth, the stress environment and geology conditions become more and more complex. The stress state in 3D space is defined by three mutually perpendicular principal stress components ( $\sigma_1$ ,  $\sigma_2$ ,  $\sigma_3$ ). Rock will exhibit different failure conditions under different stress paths. For example, with a certain minimum principal stress, researchers found that the strength of some rock increases and then decreases with the increase of intermediate principal stress. In the experimental context, many researchers (e.g. Mogi, 1979; Xu and Geng, 1985, 1989; Li and Xu, 1991; Chang and Haimson, 2000; Haimson and Chang, 2000, 2002; Chen and Feng, 2006; Mogi, 2007; Yang and Liu, 2007; Liu and Cao, 2008) conducted a large number of true triaxial tests on different

rock types such as Dunham dolomite, Solnhofen limestone, granite etc., to study their behaviour under triaxial stress conditions. They found that the strength increases and then decreases with the increase of  $\sigma_2$ .

In the theoretical context, many failure criteria (Colmenares and Zoback, 2002), such as Mohr-Coulomb, Drucker-Prager, Weibols and Cook (Wiebols and Cook, 1968), modified Wiebols and Cook (Zhou, 1994), Hoek and Brown (Hoek and Brown, 1980), Mogi 1967 and Mogi 1971 criteria (Mogi, 2007), modified Lade criterion (Ewy, 1999) etc., have been developed to fit the experimental data.

At the same time, researchers have developed many numerical models or used commercial software to study the failure processes of rocks under polyaxial stress conditions. Cai (2008) investigated the influence of the intermediate principal stress on rock fracturing and strength near excavation boundaries using a FEM/DEM combined numerical tool. Shi and Li (2009) conducted true triaxial simulation of a homogeneous rock specimen using the Mohr-Coulomb perfect plastic model in FLAC3D software and found that the end friction can lead to an apparent effect of the intermediate principal stress, even though the rock actually has no intermediate principal stress

\* Corresponding author. Tel.: +86 27 87198805.

E-mail address: pzpan@whrsm.ac.cn (P.-Z. Pan).

effect. Tang and Hudson (2010) have collected many simulation results using the RFPA code which support the general use of the EPCA code reported here for studying the emergent properties of a heterogeneous microstructure.

To summarize these studies, researchers have conducted true triaxial tests and detected the phenomenon of the intermediate principal stress effect on rock strength for some rock types. Many polyaxial yield criteria have been developed to fit this effect. By using numerical modelling, the phenomenon of the intermediate principal stress effect has been reproduced. However, the reason why the strength of some rocks firstly increases and then decreases with continued increase in the intermediate principal stress is still unclear.

Because rock is a heterogeneous material, in the study of the effect of polyaxial stress conditions on rock fracturing behaviour, the heterogeneity of rocks should be considered. The combinations of statistical theory with numerical models are thought to be appropriate for modelling the failure processes of rocks. Additionally, in polyaxial compression tests, the specimen is always loaded through some type of loading platens. Because friction exists between these loading platens and the specimen ends, in the study of the intermediate principal stress effect, such friction should also be considered.

Therefore, based on the understanding of typical intermediate stress experimental phenomena and associated theoretical analysis, a series of numerical tests were conducted to simulate the failure processes of rocks under the polyaxial compression condition using the numerical model EPCA3D (Pan et al., 2009). Two different failure criteria, i.e. the Drucker–Prager criterion, which incorporates the  $\sigma_2$  effect, and the Mohr–Coulomb criterion, which is independent of  $\sigma_2$ , were used in the meso-scopic element to study overall rock strength variation. The information generated in the rock loading process, such as deformation, failure pattern and acoustic emission etc., was collected from the EPCA3D modelling to illuminate the intrinsic behaviour that leads to the phenomenon of the intermediate principal stress effect.

## 2. Numerical tool—EPCA3D

Based on the self-organization theory of cellular automata, elasto-plastic theory, rock mechanics and statistical theory, a numerical model, EPCA3D, has been developed and the associated numerical system has been compiled in the Visual C++ environment. This system has been used to simulate the failure processes of heterogeneous rocks under uniaxial compression in previous work by the authors (Pan et al., 2009). This model contains the following basic contents: a heterogeneous material model, cellular automaton updating rules, acoustic emission definition and constitutive relation, etc.

### 2.1. Representation of heterogeneity

Geomaterials in general are heterogeneous in nature. The appropriate description of rock property is the key to study its failure mechanism. In EPCA3D model, deterministic and probabilistic approaches are used to describe rock material properties.

#### 2.1.1. Probabilistic approach

For rock specimen without naked flaws but with microcracks the random method is used to describe its heterogeneity. The physical parameters, including the Young's modulus, strength and permeability etc, are assumed to conform to certain stochastic distribution such as Weibull's or Normal distribution etc. The probability density function of Weibull's distribution (Weibull, 1951) is defined by the following equation,

$$p(x) = \begin{cases} \frac{m}{x_0} \left(\frac{x}{x_0}\right)^{m-1} \exp\left[-\left(\frac{x}{x_0}\right)^m\right], & x \geq 0 \\ 0, & x < 0 \end{cases} \quad (1)$$

where  $x$  is the parameter of the element; the scale parameter  $x_0$  is related to the average of element parameter and the parameter  $m$ , defines the shape of the distribution function.

#### 2.1.2. Deterministic approach

For rock specimen with naked flaws, deterministic method to describe the properties of rocks is used. The physical parameters of fracture are much weaker than that of rock matrix. In this case, rock matrix can be seemed as homogeneous materials. However, studies have shown that the properties of rock matrix have great influence on the crack initiation, propagation and coalescence. In this case, the random method and deterministic method will be combined to describe rock properties.

### 2.2. Cellular automaton updating rule

Cellular automaton updating rule is to describe the relationship between cell and its neighbours. The development of the updating rule is locally and only one cell is considered in the development of updating rule (Figure 1).

For an elasto-plastic mechanical process, based on the stress equilibrium equation, geometrical equation, constitutive equation and yield criterion etc, the equilibrium equation of cell  $D_i$  can be written as

$$K_{ij} \Delta u_j = \Delta F_i + \Delta F'_i \quad (2)$$

where  $K_{ij}$  is the total stiffness of cell elements on the cell node  $N_i$ . The stiffness of cell elements can be obtained from finite element method.  $\Delta F_i$  is the unbalance force induced by boundary and external conditions.  $\Delta F'_i$  is the summation of the equivalent nodal force produced by the yield cell elements (if any) in cell  $D_i$ .

The increment nodal force  $\Delta F_i^k$  on neighbouring cells can be obtained from the following equation,

$$\{\Delta F_i^k\} = [B_{im}^j]^T \{\Delta u_m\} \quad (3)$$

where  $B_{im}^j$  is cell element stiffness.

Each cell conforms to the same updating rule. The process of the change of force  $\Rightarrow$  the change of displacement  $\Rightarrow$  the change of force  $\Rightarrow \dots$  will be transferred among cells in the system. The system will attain its static equilibrium state when the self-organization phenomenon of  $\Delta u_i \rightarrow 0$  or  $\Delta F_i + \Delta F'_i \rightarrow 0$  appears.

It is apparent that, in the modeling, no global stiffness but local cell stiffness is used. Since the mechanical parameters of cell element may change with the accumulation of damage in the failure process, the cellular automaton technique based on localization theory makes its state updating more conveniently.

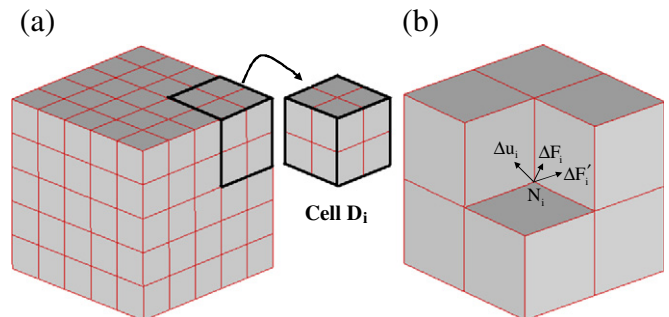


**Fig. 1.** EPCA3D model. (a) Three-dimensional domain to be solved and (b) one three-dimensional cell.

### 2.3. Polyaxial yield criteria

In the EPCA3D model, different yield criteria, modified Lade criterion, modified Wiebels-Cook, Mogi 1971, Hoek-Brown, Mohr-Coulomb and Drucker-Prager etc., can be considered. Of these criteria, the Mohr-Coulomb and Drucker-Prager criteria (Owen and Hinton, 1980) are widely used for the prediction of rock-like materials' strengths by the researchers.

#### 2.3.1. Mohr-Coulomb yield criterion

The Mohr-Coulomb theory is often used to characterise the response of brittle materials, such as rock, or concrete, to shear stress as well as normal stress. It applies to materials for which the compressive strength far exceeds the tensile strength. The yield function takes the following form,

$$F(\sigma) = \frac{1}{2}(\sigma_1 - \sigma_3) + \frac{1}{2}(\sigma_1 + \sigma_3)\sin\varphi - c\cos\varphi = 0 \quad (4)$$

where  $c$  is the cohesion,  $\varphi$  is the frictional angle. The yield surface of this criterion is a right hexagonal pyramid equally inclined to the principal stress axes. The intersection of this surface with the  $\pi$  plane is a hexagon.

For the non-associated plastic flow rule,  $Q \neq F$ . For the sake of simplicity,  $Q$  can be chosen in the same form as  $F$ . Substituting the friction angle  $\varphi$  in  $F$  as the dilation angle  $\psi$ , we have,

$$Q(\sigma) = \frac{1}{2}(\sigma_1 - \sigma_3) + \frac{1}{2}(\sigma_1 + \sigma_3)\sin\psi - c\cos\psi = 0. \quad (5)$$

If  $\psi = 0$ , no volumetric dilation occurs, even though the rock mass fails in shear. If  $\psi = \varphi$ , the maximum volumetric dilation occurs when the rock mass fails in shear, in which the associated flow rule is used.

#### 2.3.2. Drucker-Prager yield criterion

The Drucker-Prager yield criterion was introduced to deal with the plastic deformation of rock and soil materials. It is a pressure-dependent model for determining whether a material has failed or undergone plastic yield. The yield function takes the following form (Chen, 1982),

$$F = a_\varphi I_1 + \sqrt{J_2} - k = 0 \quad (6)$$

where  $a_\varphi$  and  $k$  are material constants, both of which are related to the cohesion and frictional angle (see Eqs. (5) and (6)).

The yield surface of this criterion is a right-circular cone in principal stress space. On the  $\pi$  plane, the yield surface is a circle.

For a perfect elasto-plastic material, the plastic potential function can be expressed as,

$$Q = a_\psi I_1 + \sqrt{J_2} - k = 0. \quad (7)$$

In terms of the yield surfaces, the Mohr-Coulomb hexagonal yield surface is not smooth but has corners. These corners of the hexagon can cause numerical difficulty in its application to plasticity theory since the normal vector to the yield surface needs to be calculated. The Drucker-Prager criterion can be viewed as a smooth approximation to the Mohr-Coulomb criterion to avoid such difficulty; also the Drucker-Prager criterion may be made to match the Mohr-Coulomb criterion by adjusting the size of the cone. If the Drucker-Prager circle is made to agree with the outer apices of the Mohr-Coulomb hexagon (Figure 2a) (the circumscribed Drucker-Prager criterion), i.e. the two

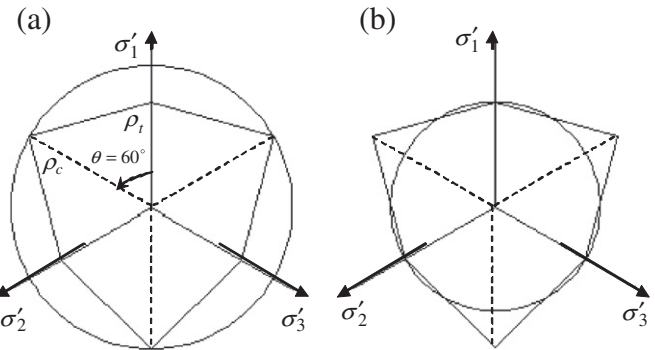


**Fig. 2.** Relation between Mohr-Coulomb and Drucker-Prager criteria. (a) Drucker-Prager circle is made to agree with the outer apices of the Mohr-Coulomb hexagon (circumscribed Drucker-Prager criterion). (b) The Drucker-Prager cone is made to inscribe the Mohr-Coulomb hexagon (inscribed Drucker-Prager criterion).

surfaces are made to coincide along the compressive meridian  $\rho_c$ , then the constants  $\alpha$  and  $k$  of the Drucker-Prager criterion are related to the parameters  $c$  and  $\varphi$  of the Mohr-Coulomb criterion as

$$\alpha_\varphi = \frac{2 \sin\varphi}{\sqrt{3}(3 - \sin\varphi)}, k = \frac{6c \cos\varphi}{\sqrt{3}(3 - \sin\varphi)}. \quad (8)$$

The cone corresponding to the constants in the above equation circumscribes the hexagonal pyramid. The Drucker-Prager cone may be made to inscribe the Mohr-Coulomb hexagon as well, passing through the tensile meridian  $\rho_t$  (Figure 2b) (inscribed Drucker-Prager criterion). In such a case, the constants of the two criteria are related by

$$\alpha_\varphi = \frac{2 \sin\varphi}{\sqrt{3}(3 + \sin\varphi)}, k = \frac{6c \cos\varphi}{\sqrt{3}(3 + \sin\varphi)}. \quad (9)$$

#### 2.4. Simulation of post-peak behaviour

The observed mechanical response of rocks can be categorized through three stages of the complete stress-strain curve. These stages are the pre-peak region (pre-failure), peak (maximum strength) and post-peak region (post-failure) (Hudson and Harrison, 1997). The failure of rock in this context happens at the peak stress when the maximum strength of the rock is reached. In the post-peak region, different rock can present different behaviour, such as hardening, perfect plasticity, strain softening or brittleness, etc. These different types of behaviour are determined by many factors, including the rock properties and the environment.

In plasticity theory, a post-failure parameter  $h$  is introduced to account for the fact that the post-failure behaviour of materials during yielding is not perfectly plastic, and most often involves a decrease (weakening) or an increase (strengthening) in resistance. This weakening or strengthening is a function of plastic strain and is not uniquely defined by the stresses. An effective plastic strain parameter,  $\bar{\varepsilon}^p$  is used to represent the plastic strains. This parameter represents the current and the history of plastic strain (accumulated damage), expressed as follows,

$$\bar{\varepsilon}^p = \int \sqrt{\frac{2}{3} (d\varepsilon_1^p d\varepsilon_1^p + d\varepsilon_2^p d\varepsilon_2^p + d\varepsilon_3^p d\varepsilon_3^p)} \quad (10)$$

where  $d\varepsilon_1^p$ ,  $d\varepsilon_2^p$ ,  $d\varepsilon_3^p$  are the increments of principal plastic strain.

It is known that, for brittle failure of rock, at low confinement, the cohesive strength initially governs the mobilized strength and it is gradually replaced by the frictional strength when the cohesion is consumed. The CWFS (cohesion weakening and frictional strengthening)

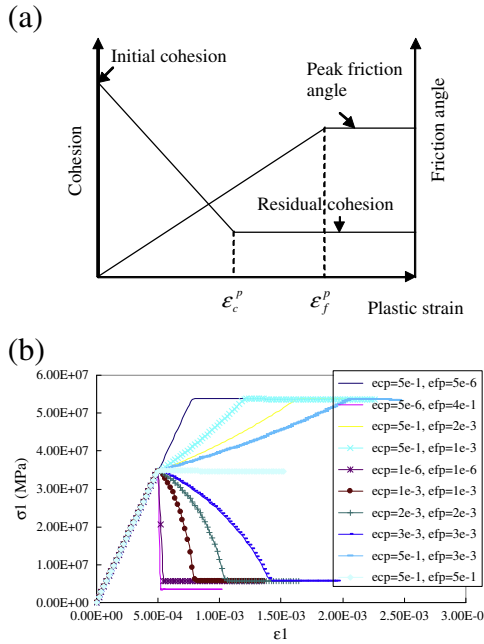


**Fig. 3.** (a) Cohesion weakening and friction strengthening (CWFS) model and (b) EPCA3D simulated complete  $\sigma_1 - \epsilon_1$  curves by considering different combinations of  $\epsilon_c^p$  and  $\epsilon_f^p$  in the CWFS model.

model (Martin, 1997; Hajabdolmajid, 2001) can capture this characteristic of rock brittle failure (Figure 3a). In this model, the cohesion and friction angle are functions of the plastic strain; the cohesion is weakened and the friction is strengthened linearly according to the plastic strain level. By selecting the appropriate magnitude of  $\epsilon_c^p$  and  $\epsilon_f^p$ , different post-peak deformation behaviour can be obtained. For example, if  $\epsilon_c^p$  is very small or zero and  $\epsilon_f^p$  is very large, the stress will drop immediately to the rock's residual strength surface once its peak strength is reached. In this case, the rock behaves in a brittle manner. If both  $\epsilon_c^p$  and  $\epsilon_f^p$  are very large, the rock will behave perfectly plastically. If  $\epsilon_c^p$  is very large and  $\epsilon_f^p$  is very small, the rock will behave in strain hardening manner (Figure 3b).

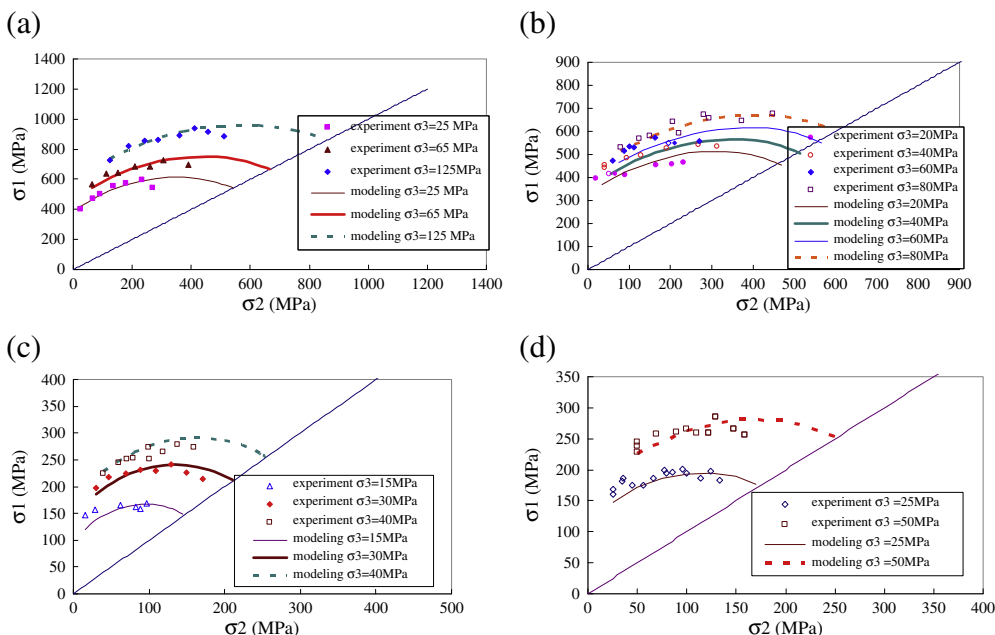


**Fig. 4.** The relation between  $\sigma_2$  and  $\sigma_3$  of different rock types (curves are EPCA3D results. Discrete points are experimental results). (a) Dunham dolomite; (b) Solenhofen limestone; (c) Shirahama sandstone and (d) Yuubari shale.

Therefore, in the failure process of brittle rock materials, there is an initial yield surface and a residual yield surface. For the Mohr-Coulomb and Drucker-Prager criteria, i.e. Eqs. (4) and (6), the initial yield surface is controlled by  $c_i$ ,  $\varphi_i$ . The residual yield surface is controlled by  $c_r$ ,  $\varphi_r$ . In cohesive weakening and frictional strengthening process model, by assigning certain  $\epsilon_c^p$  and  $\epsilon_f^p$ , there would be many successive yield surfaces between the initial yield surface and residual yield surface.

Therefore, EPCA3D has the ability to simulate different behaviours such as brittle failure, strain softening, plasticity and strain hardening of rocks (Figure 3b). In Fig. 4, EPCA3D is used to simulate the failure process of different rock types (Dunham Dolomite, Solenhofen Limestone, Shirahama sandstone and, Yuubari shale) under different true triaxial compressions by considering different minimum principal stresses. It is found that the modeling results are quite comparable with experimental data, which also validates the EPCA3D code.

### 3. Rock fracturing simulation under polyaxial stress conditions

#### 3.1. Numerical model and mechanical parameters

A prismatic rock specimen with side length 50 mm and height 100 mm is discretized into a system composed of 3D cell elements. The parameters used in the EPCA3D modelling are shown in Table 1. The selection of the parameters reflects a type of hard rock, i.e. a brittle heterogeneous rock, but not any geologically specific rock type.

In modelling a triaxial compression process,  $\sigma_1$ ,  $\sigma_2$  and  $\sigma_3$  are applied to the specimen boundaries simultaneously step by step. When  $\sigma_3$  reaches the prescribed value,  $\sigma_3$  is kept constant and  $\sigma_1$  and  $\sigma_2$  continue to be applied on the boundaries. If  $\sigma_2$  reaches the prescribed value,  $\sigma_2$  will be kept constant and the stress on  $\sigma_1$  is continually applied on the boundary until the rock specimen fails. In the application of the confining stress, we use the stress loading control method to apply the stress on the simulated rock boundaries ( $\sigma_1$ ,  $\sigma_2$  and  $\sigma_3$ ). When  $\sigma_2$  reaches its prescribed value, the stress loading control method is replaced by the strain loading control method in the  $\sigma_1$  direction. By doing so, the complete stress-strain curves can be successfully obtained.

**Table 1**  
Parameters used in EPCA3D modelling.

Parameters	Value	Parameters	Value
Young's modulus ( $E$ )	70 GPa	Poisson's ratio ( $\nu$ )	0.26
Initial cohesion ( $c_i$ )	10 MPa	Residual cohesion ( $c_r$ )	1 MPa
Initial friction angle ( $\varphi_i$ )	30°	Residual frictional angle ( $\varphi_r$ )	49°
Homogeneous index ( $m$ )	4	CA iteration precision ( $\eta$ )	1e–12
Seed parameter ( $s$ )	10	Axial loading speed ( $d$ )	1e–6 m/step
Tolerance ( $\kappa$ )	0.01	$\varepsilon_p^p$	0.4
$\varepsilon_c^p$	5e–6		

### 3.2. Homogeneous case

EPCA3D is firstly used to simulate the failure processes of homogeneous rocks under a true triaxial compression condition using the Drucker–Prager and Mohr–Coulomb criteria. The boundary stresses are applied on the boundaries directly – so that there is no friction between the rock specimen's ends and the loading platen. In the simulation, the initial cohesion is 10 MPa, residual cohesion 1 MPa, initial friction angle 30°, and residual friction angle 49°. The Young's modulus is 70 GPa and the Poisson's ratio is 0.26. Two levels of  $\sigma_3$  ( $\sigma_3 = 0$  MPa and 10 MPa) are considered. Fig. 5 shows the EPCA3D simulated results plotted in  $\sigma_1$ – $\sigma_2$  space. It is clear that the strength of homogeneous rock is greatly influenced by  $\sigma_2$  when the Drucker–Prager criterion is used. It increases firstly and then decreases with the increment of  $\sigma_2$ . Since the Mohr–Coulomb criterion does not consider the effect of  $\sigma_2$ , the simulated strength of homogeneous rock remains constant no matter what the magnitude of  $\sigma_2$  is. In this modelling, the perfect loading condition (i.e. no friction between the loading platens and specimen's ends) is considered, so the homogeneous rock specimen fails with each cell element in the plastic state when the stress reaches the peak strength.

### 3.3. Heterogeneous case

Rock is a naturally heterogeneous material; it follows that the failure behaviour of rock is likely to be greatly influenced by this heterogeneity. Thus, in the failure process modelling of rocks under polyaxial stress conditions, heterogeneity is an important factor to be considered. Therefore, the Drucker–Prager criterion is firstly used in EPCA3D modelling to simulate the failure processes of heterogeneous rocks under true triaxial compression with consideration of different  $\sigma_3$  values. The influence of  $\sigma_2$  on the deformation and failure processes of rocks is shown in Figs. 6 and 7, in which  $\sigma_2 = 10$  MPa and  $\sigma_2 = 50$  MPa are considered, respectively. When  $\sigma_2 = \sigma_3$ , the lateral deformations in both the  $\varepsilon_2$  and  $\varepsilon_3$  directions are almost the same and represent a state of expansion (Figure 6a). Since  $\sigma_1 = \sigma_2 = \sigma_3$ , which means that this is a hydrostatic state, there are almost no internal elements failing during the process of applying  $\sigma_2$ . Failure

initiation occurs when further stress is subjected in the  $\sigma_1$  direction. The failure cell elements are randomly distributed, firstly in the specimen and then a shear failure zone is formed finally (Figure 6b). With the increase of  $\sigma_2$ , the expansive deformation in the  $\varepsilon_2$  direction is restricted, as can be seen from Fig. 7a, in which  $\varepsilon_2$  is in compaction mode, while  $\varepsilon_3$  is in expansion mode. From Fig. 7b, it is clear that there are internal elements failed during the process of applying  $\sigma_2$ . With the increase of stress in the axial direction, the 'cracks' continue to propagate. Most of the 'cracks' or the plane formed by the accumulated failure cell elements are found in the direction parallel to  $\sigma_2$ , which is different from that with lower  $\sigma_2$  (Figure 6b).

The EPCA3D simulated  $\sigma_1$ – $\sigma_2$  relations using the Drucker–Prager criterion are plotted in Fig. 8. From these results, we note that the EPCA3D simulation has reproduced the typical manifestation of the intermediate principal stress effect (Mogi, 1979, 2007) concerning heterogeneous rock strength. The results obtained for the heterogeneous case have the same trend as the homogeneous case shown in Fig. 5. It may be thought that the results in Fig. 8 are inevitable because we use the criterion (Drucker–Prager) that does inherently reflect the intermediate principal stress effect. In other words, the fact that the simulated results reflect the  $\sigma_2$  effect follows from the selection of the Drucker–Prager yield criterion. But, for heterogeneous rocks, the mechanism of the intermediate principal stress effect is more complex: the results in Fig. 8 are also a function of the rock heterogeneity.

In order to demonstrate the influence of heterogeneity on the  $\sigma_2$  effect, the Mohr–Coulomb criterion, which is independent of  $\sigma_2$  for homogeneous rock (Figure 5), was used for the elements in the EPCA3D modelling. Parameters used in the modelling are shown in Table 1. The simulated results are presented in Fig. 9. It is found that the strength of the rock specimen increases firstly and then decreases with the increase of the intermediate principal stress. This indicates that, although we use a criterion that does not consider the  $\sigma_2$  effect (i.e. the Mohr–Coulomb criterion) for internal cell element in the modelling of the heterogeneous rock failure process, the typical emergent phenomenon for the whole sample of the intermediate principal stress effect on rock strength is also reproduced.

From the above results, two questions are evident: one concerns why the strength increases with an increase in  $\sigma_2$ ; the other concerns why the rock strength decreases with an increase in  $\sigma_2$  after  $\sigma_2$  has reached a certain value. If these two questions can be answered, the mechanism of the  $\sigma_2$  effect on rock strength should be clear.

Fig. 10 shows that with the same stress in the  $\sigma_1$  direction, the axial strain  $\varepsilon_1$  decreases with the increase of  $\sigma_2$  in the pre-peak region. That is to say, the  $\sigma_2$  restrains the deformation in the  $\sigma_1$  direction when  $\sigma_2$  is low. As a result, the internal elements (cell elements) that may fail for a lower  $\sigma_2$  will be in an elastic state for higher values of  $\sigma_2$ . If we wish to make these internal elements fail for higher  $\sigma_2$ , further stress in the  $\sigma_1$  direction should be exerted, which will lead to a rock strength higher than for the lower  $\sigma_2$ . This can also be seen in Fig. 9, in which the  $\sigma_1$  and accumulated AE counts before the peak stress with respect to  $\sigma_2$  are plotted.

It should be noted that the simulated AE events are not actual events, but the counts of internal elemental failure points. However, it does simulate the actual failure of rocks. The definition of AE has been described in detail in previous papers by the authors (Feng et al., 2006 and Pan et al., 2009).

It is seen that, for  $\sigma_3 = 10$  MPa (Figure 9a), the accumulated AE counts are 7722 (generated through the individual elemental cell failures) when  $\sigma_2 = 10$  MPa before the peak stress. However, when  $\sigma_2 = 15$  MPa, the accumulated AE counts reduce to 3354 before the peak stress. Note that the number of AE counts is directly linked to the number of internal failure elements; therefore, the number of failed cell elements (internal elements) when  $\sigma_2 = 10$  MPa is more than that when  $\sigma_2 = 15$  MPa. As a result, the rock strength is higher ( $\sigma_1 = 48.1$  MPa) for  $\sigma_2 = 15$  MPa than that for  $\sigma_2 = 10$  MPa

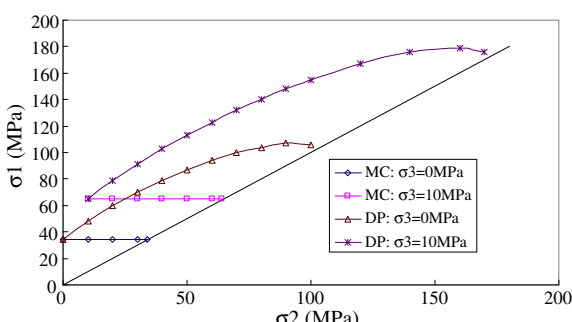
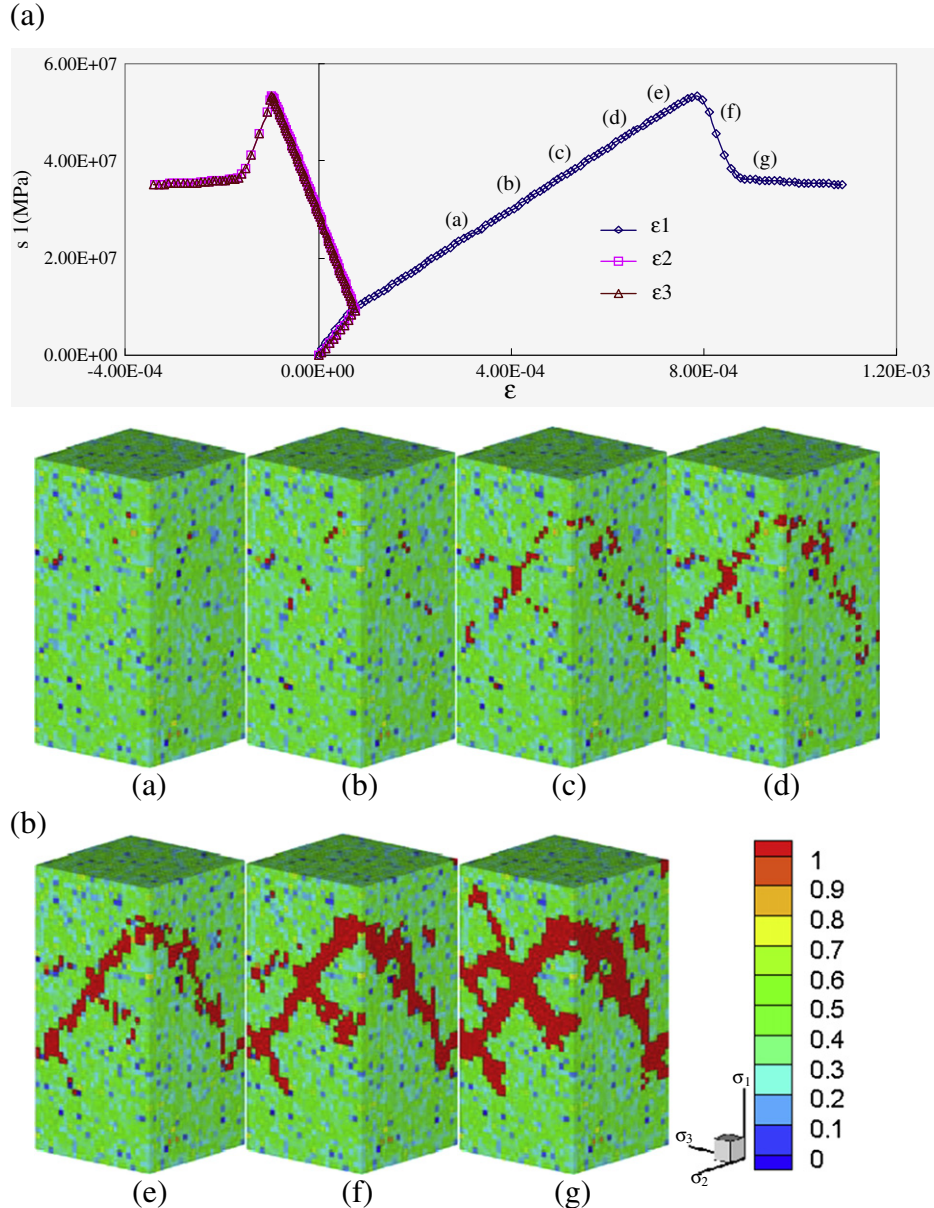


Fig. 5. EPCA3D simulated results for the relation between  $\sigma_1$  and  $\sigma_2$  for a homogeneous rock specimen using the Drucker–Prager criterion and Mohr–Coulomb criterion.



**Fig. 6.** EPCA3D simulated results when  $\sigma_2 = \sigma_3 = 10$  MPa using the Drucker–Prager criterion (a) relation of  $\epsilon_1$ ,  $\epsilon_2$  and  $\epsilon_3$  with respect to  $\sigma_1$  (b) failure process.

( $\sigma_1 = 44.5$  MPa). In other words, the onset of failure is delayed with the increase of  $\sigma_2$  when  $\sigma_2$  is not sufficiently large, which leads to the increase in the rock strength. For  $\sigma_3 = 20$  MPa, the similar phenomenon can be found in Fig. 9b.

Fig. 11 presents one of the EPCA3D simulated complete  $\sigma_1 - \epsilon_1$  curves and the AE– $\epsilon_1$  relation during the failure process of heterogeneous rock using the Mohr–Coulomb criterion with the application of  $\sigma_2 = 35$  MPa and  $\sigma_3 = 10$  MPa. It is clear that, although most of the AE counts occur around the peak stress, in the process of applying  $\sigma_2$ , there are also a few AE counts produced, indicating that there are cell elements failing in the process of applying  $\sigma_2$ , if  $\sigma_2$  is large enough.

In uniaxial and triaxial compression tests, there are different loading methods (Pan et al., 2006) (in the axial direction), such as the constant stress loading method, constant strain loading method and the linear combination of stress and strain loading method etc., to control the failure processes of rocks. By using the constant strain loading method and the linear combination of stress and strain loading method, the complete stress–strain curves of rocks can be traced. However, how does the stress decrease during the failure processes for heterogeneous

brittle rocks, which behaves as strain softening in the uniaxial condition or triaxial condition with low confinement? Take the uniaxial compression (constant strain as the control variable) failure process of brittle rock as an example: in the pre-peak region: if there are no internal elements that failed, the stress–strain curve will be linear; however, for heterogeneous brittle rock, with the increase of axial stress, the onset of failure will occur and the stress–strain curve will deviate from the linear state. At this stage, because the number of failed internal elements is small, the axial stress can be increased. Once the number of failed internal elements reaches a certain value, the rock will manifest stress reduction in the complete stress–strain curve. The same circumstance happens during the true triaxial compressive failure process of heterogeneous brittle rocks. In the process of applying  $\sigma_2$ , if there are too many internal elements that failed, there is no need for a too high application of  $\sigma_1$  to cause the stress in the rock specimen to decrease. This can be explained again in Fig. 9a. From  $\sigma_2 = 15$  MPa, the accumulated AE counts begins to increase, but the rock strength does not decrease with the increase of  $\sigma_2$ . However, the extent of rock strength increase is reduced with the increase of  $\sigma_2$ . When  $\sigma_2 = 20$  MPa, the accumulated

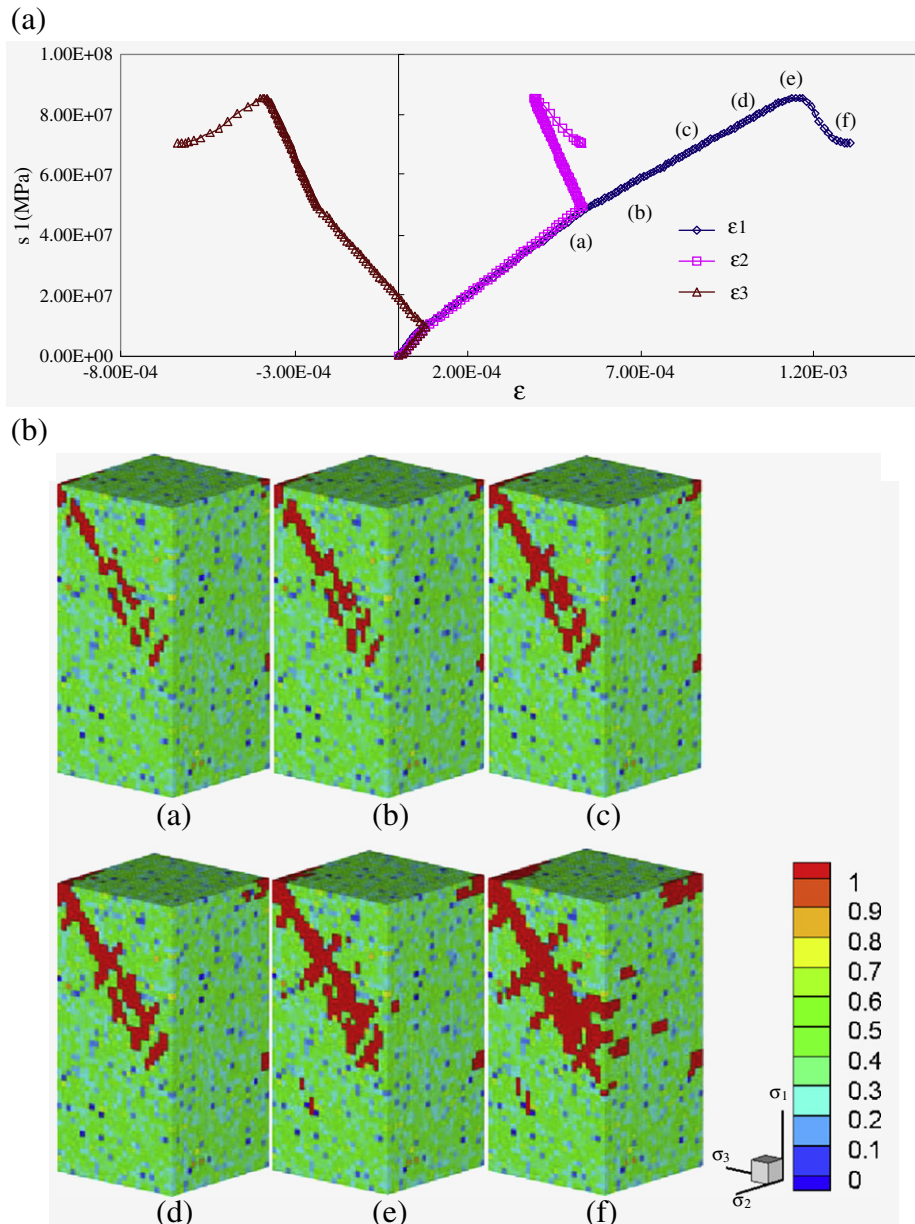


**Fig. 7.** EPCA3D simulated results when  $\sigma_2=50$  MPa,  $\sigma_3=10$  MPa using the Drucker–Prager criterion (a) relation of  $\epsilon_1$ ,  $\epsilon_2$  and  $\epsilon_3$  with respect to  $\sigma_1$  (b) failure process.

AE counts are 8300, the rock strength attains its peak strength at 49.2 MPa. After that, with the increase of the accumulated AE counts due to the increase of  $\sigma_2$ , the rock strength decreases gradually.

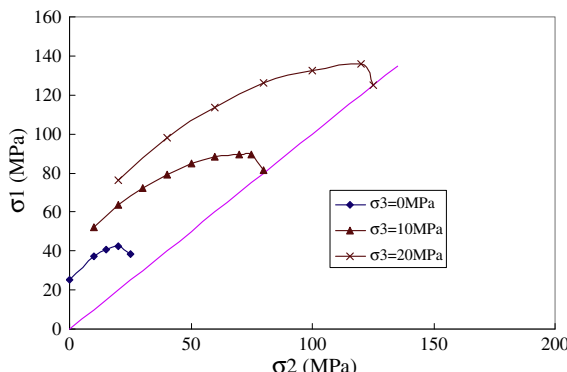


**Fig. 8.** EPCA3D simulated results using Drucker–Prager criterion.

Therefore, for heterogeneous rock, in Fig. 8, not all of the contribution to the phenomenon of the  $\sigma_2$  effect comes from the selection of the elemental failure criterion (Drucker–Prager criterion), but a component is due to the heterogeneity of the rock specimen. While in Fig. 9, this phenomenon is rooted in the heterogeneity of the rock specimen completely. Fig. 9 also indicates that the extent of rock strength reduction when  $\sigma_2$  exceeds a certain value is weakened with the increment of  $\sigma_3$ .

Fig. 12 shows the comparisons between homogeneous and heterogeneous results for  $\sigma_3=10$  MPa. It is found that with the same  $\sigma_2$ , the strength in the  $\sigma_1$  direction is much higher for the homogeneous case than that for the heterogeneous case.

To truly access the influence of heterogeneity on  $\sigma_2$  effect, different homogeneous indices, i.e.  $m=2.0, 4.0, 6.0$ , and the same homogeneity index ( $m=4.0$ ) but different spatial distributions, i.e.  $s=5, 10, 15$ , are used to create different simulated rock samples. Using the Mohr–Coulomb criterion, these samples are used to simulate the failure process with different  $\sigma_2$ , by considering  $\sigma_3=10$  MPa. From Fig. 13a, the rock strength in the  $\sigma_1$  direction increases with the

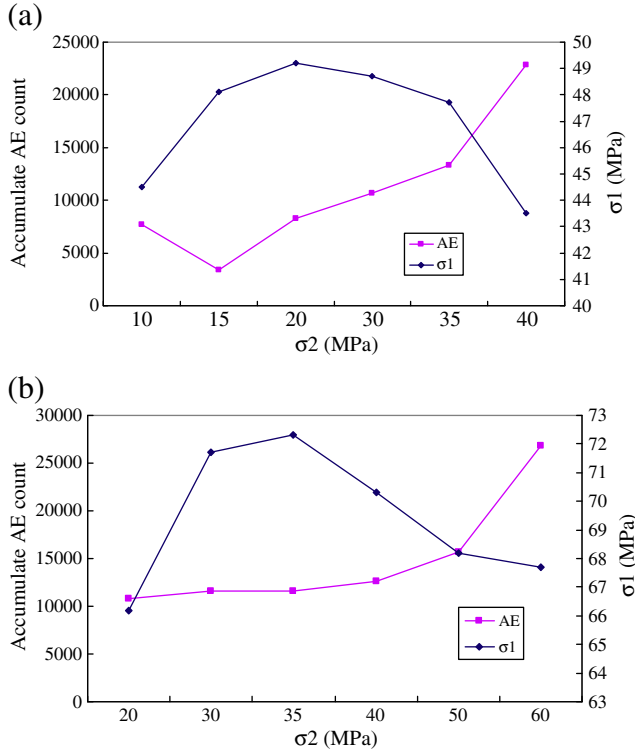


**Fig. 9.** EPCA3D simulated  $\sigma_1$  and accumulated AE counts before the peak stress with respect to  $\sigma_2$  using the Mohr-Coulomb criterion. (a)  $\sigma_3 = 10$  MPa and (b)  $\sigma_3 = 20$  MPa.

increase of the homogeneity index. For a different homogeneity index, the same trend, i.e. rock strength firstly increases and subsequently decreases with the increase of intermediate principal stress is still found. With the same homogeneity index but different spatial random distribution, the rock strengths have little differences (Figure 13b).

#### 3.4. The effect of the loading platen on rock strength

In the above simulations, the boundary stresses are applied directly on the boundaries. The results are not affected by friction that exists in some physical experiments between the loading platen and the specimen's ends. This is one of the advantages of the numerical method; it can simulate perfect loading conditions. However, in the real experimental situation some friction between the platens and the rock specimen's ends is inevitable. Consequently, a heterogeneous stress field will be produced in the loading process even though the rock specimen itself is

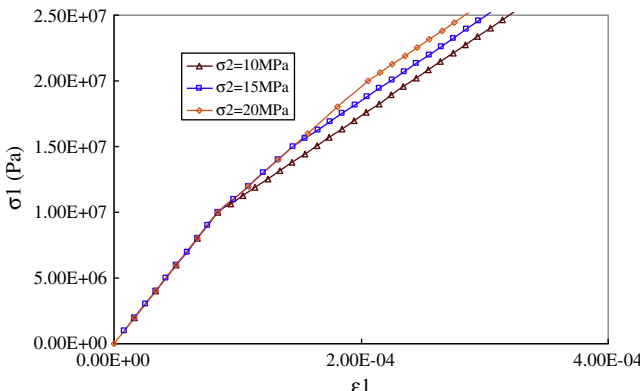


**Fig. 10.** EPCA3D simulated  $\sigma_1 - \epsilon_1$  relation before the peak stress using the Mohr-Coulomb criterion ( $\sigma_3 = 10$  MPa).

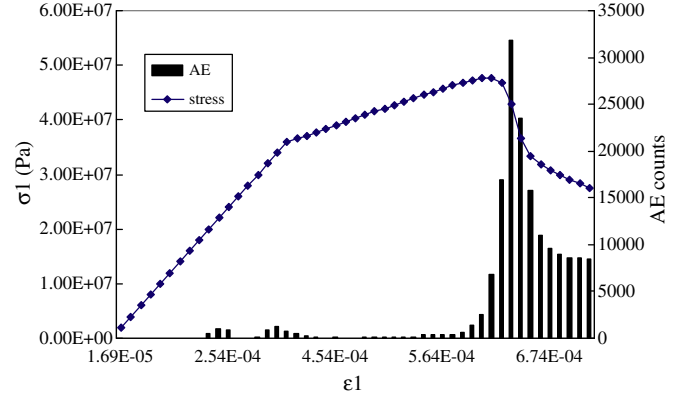


**Fig. 11.** EPCA3D simulated complete  $\sigma_1 - \epsilon_1$  and AE –  $\epsilon_1$  relation during the failure process modelling of heterogeneous rock using the Mohr-Coulomb criterion ( $\sigma_2 = 35$  MPa and  $\sigma_3 = 10$  MPa).

homogeneous. Shi and Li (2009) studied this phenomenon using a Mohr-Coulomb perfect plastic model in Flac3D software.

In this section, EPCA3D is used to simulate the failure processes of a rock specimen with consideration of the loading platen effect. Some of the physical parameters are shown in Table 1 but a homogeneous rock specimen is considered. The Young's modulus of steel platen is 120 GPa (113–157 GPa for steel) and the Poisson's ratio is 0.25 (0.23–0.27 for steel). Fig. 14 shows the result simulated by EPCA3D with  $\sigma_3 = 0$  MPa. For the perfect condition of no platen effect (i.e. no ends' frictional existence), the simulated failure stress is independent of  $\sigma_2$  (see Figure 5). Due to the existence of friction between the loading platens and specimen's ends, the friction increases with the increase of  $\sigma_2$ . This increases the heterogeneous distribution of stress in the specimen, which in turn causes the rock strength to increase with the increase of  $\sigma_2$ .

However, for a situation of low  $\sigma_3$  or  $\sigma_3 = 0$ , the increase of rock strength is not unbounded. After  $\sigma_2$  reaches a certain value, the rock

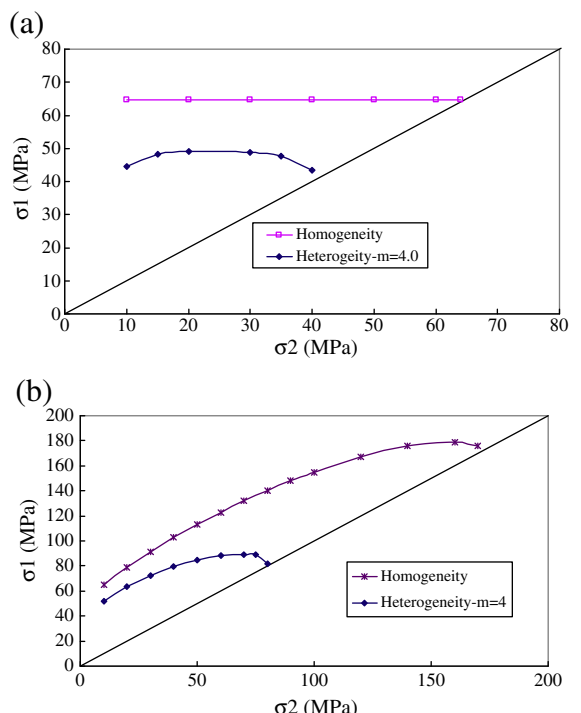


**Fig. 12.** Comparisons between homogeneous and heterogeneous results with  $\sigma_3 = 10$  MPa. (a) Mohr-Coulomb criterion; (b) Drucker-Prager criterion.

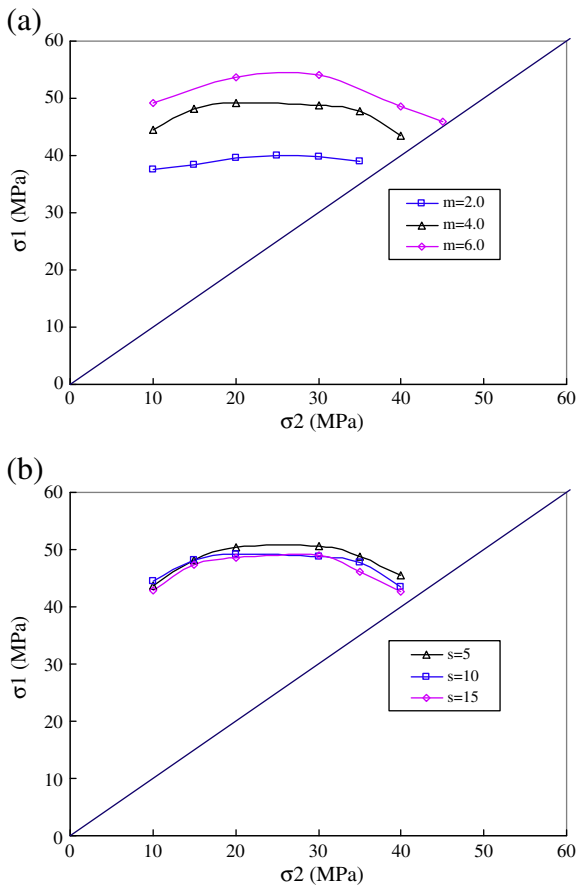


**Fig. 13.** Relation of  $\sigma_1 - \sigma_2$  with different heterogeneity ( $\sigma_3 = 10$  MPa). (a) different homogeneous indices,  $m = 2.0, 4.0, 6.0$ . (b) the same homogeneity index  $m = 4.0$ , different spatial random seed,  $s = 5, 10, 15$ .

strength begins to decrease (Figure 14a), which presents the same trend shown in Fig. 9. In this case, compared with the strength and the accumulated AE counts before peak stress, a moderate magnitude of  $\sigma_2$  also delays the onset of failure, which makes the strength increase. When  $\sigma_2$  exceeds a certain value, large number of internal elements fails in the pre-peak region and the strength of rock begins to decrease. Due to the existence of friction, the stress in rock specimen is heterogeneously distributed. As a result, the final failure pattern (Figure 14b) becomes more complex than that under the perfect loading condition for homogeneous rocks.

The decrease of rock strength with the increment of  $\sigma_2$  when  $\sigma_2$  exceeds a certain value is dependent on the magnitude of the

minimum principal stress  $\sigma_3$ . For low or zero minimum principal stress, the rock behaves in a brittle fashion. With the increase in  $\sigma_3$ , the rock behaviour changes from brittle to ductile or hardening. As a result, the extent of rock strength reduction will be less with the increment of  $\sigma_2$ . If the value of  $\sigma_3$  is large enough, the rock will behave in a ductile or even hardening manner, its strength will not decrease, and the previous trend will be reversed (Figure 15).

#### 4. Conclusions

- 1) In the failure processes of rocks subjected to polyaxial stress conditions, there are two interesting questions: (1) why does the rock strength increase with an increase in the intermediate principal stress? and (2) why does the rock strength decrease with an increase in the intermediate principal stress when the intermediate principal stress reaches a certain value? By using the numerical modelling system EPCA3D, these two questions have been answered numerically.
- 2) It is found that the heterogeneous stress field in a natural rock specimen during the loading process is one of the reasons that leads to the intermediate principal stress effect. There are many factors that can produce such a heterogeneous stress field, the heterogeneity of the rock specimen and the friction between the loading platen and the specimen's ends being the most important. In this paper, these two different factors have been considered in the EPCA3D modelling. However, in real situation, the phenomenon of the  $\sigma_2$  effect may be induced by a combination of these factors, i.e. the overall failure behaviour, as the strength, deformation and failure process of the rock specimen in a physical experiment are greatly influenced by the properties of the rock itself and the boundary conditions.
- 3) It is concluded that, for a brittle rock specimen, a moderate intermediate principal stress delays the onset of failure propagation, which leads to the increase of the rock strength. However, once the intermediate principal stress reaches a certain value, 'cracks' will be formed during the process of applying the intermediate principal stress. It is the number of failed cell elements in the pre-peak region that leads to the decrease of rock strength. The decrease of rock strength when  $\sigma_2$  exceeds this certain value is a function of the value of the minimum principal stress, due to the rock transferring from brittle to ductile or hardening behaviour. Due to the heterogeneous stress field produced by the rock heterogeneity and the loading platen effect, even though the criterion for the elements in the EPCA is independent of  $\sigma_2$  (e.g. using the Mohr-Coulomb criterion), the phenomenon of the  $\sigma_2$  effect is an emergent property for the whole specimen and can also be reproduced numerically.
- 4) It should be noted that in this study the Drucker-Prager or Mohr-Coulomb elasto-brittle-plastic model is assigned to each internal

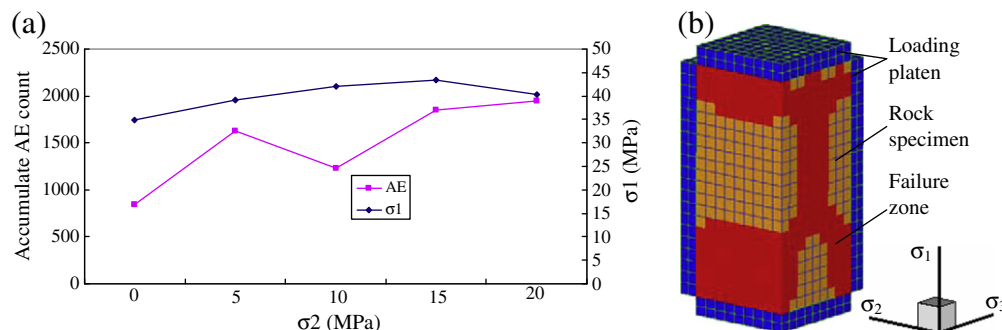


**Fig. 14.** EPCA3D simulated results when  $\sigma_3 = 0$  MPa by consideration of the loading platen effect for a homogeneous rock specimen. (a) Relation of  $\sigma_1 - \sigma_2$  and  $\sigma_2$ -accumulated AE counts before the peak stress and (b) Failure pattern (blue colour represents loading platens, orange colour represents rock specimen, red colour represents failure zone).

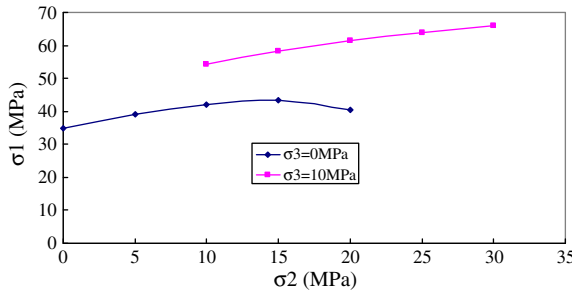


Fig. 15. EPCA3D simulated  $\sigma_1$ – $\sigma_2$  relation with different  $\sigma_3$  for homogeneous rocks with consideration of the loading platen effects.

element. That is to say, in the above modelling, we use  $\varepsilon_c^p = 5e - 6$  and  $\varepsilon_p^p = 0.4$  (see Table 1), which means that each cell element has pure brittle properties, because, once its stress reaches the peak strength it will drop to its residual strength surface in the uniaxial compression condition. Therefore, in this modelling, we assume that the rock specimen is composed of brittle material. If other sets of  $\varepsilon_c^p, \varepsilon_p^p$  are chosen for assuming that the rock is a ductile or hardening material, the rock strength will increase, but may not decrease with the increase of  $\sigma_2$  in the modelling. For example, Shi and Li (2009) used a perfect plastic model in Flac3D modelling and found that the rock strength increases with the increase of  $\sigma_2$  and never decreased, even though  $\sigma_2$  is large enough. Moreover, even though the rock behaves in a brittle manner under uniaxial compression or triaxial compression with low minimum principal stress, it may behave in a ductile or strain hardening manner under triaxial compression with a high applied minimum principal stress. In this case, the rock strength will increase, but also may not decrease with the increase in  $\sigma_2$ .

5) The EPCA3D system provides a robust and realistic ability for rock fracturing simulation of polyaxial stress conditions. However, further improvement of this system, including a parallel version, other failure criteria, and correlation of the material heterogeneity parameters, etc., is required to better simulate the observed rock fracturing process with great reality and to provide full sensitivity studies. This will be the subject of future papers

## Acknowledgements

This work was supported by a grant from the National Basic Research Program of China (No. 2010CB732006) and the National Natural Science Foundation of China (Nos. 10972231, 50709036).

## References

- Cai, M., 2008. Influence of intermediate principal stress on rock fracturing and strength near excavation boundaries—insight from numerical modeling. International Journal of Rock Mechanics & Mining Sciences 45 (5), 763–772.

- Chang, C., Haimson, B.C., 2000. True triaxial strength and deformability of the KTB deep hole amphibolite[J]. Journal of Geophysical Research 105 (8), 18999–19013.
- Chen, W.F., 1982. Plasticity in Reinforced Concrete. McGraw-Hill Company.
- Chen, Jingtao, Feng, Xiating, 2006. True triaxial experimental study on rock with high geostress. Chinese Journal of Rock Mechanics and Engineering 25 (8), 1537–1543.
- Colmenares, L.B., Zoback, M.D., 2002. A statistical evaluation of intact rock failure criteria constrained by polyaxial test data for five different rocks. International Journal of Rock Mechanics & Mining Sciences 39 (6), 695–729.
- Ewy, R.T., 1999. Wellbore-stability predictions by use of a modified Lade criterion. SPE Drill Completion 14 (2), 85–91.
- Feng, X.T., Pan, P.Z., Zhou, H., 2006. Simulation of the rock microfracturing process under uniaxial compression using an elasto-plastic cellular automaton. International Journal of Rock Mechanics & Mining Sciences 43 (7), 1091–1108.
- Haimson, B.C., Chang, C., 2000. A new true triaxial cell for testing mechanical properties of rock, and its use to determine rock strength and deformability of Westerly granite. International Journal of Rock Mechanics & Mining Sciences 37 (1–2), 285–296.
- Haimson, B.C., Chang, C., 2002. True triaxial strength of KTB amphibolite under borehole wall conditions and its use to estimate the maximum horizontal in-situ stress. Journal of Geophysical Research 107 (B10), 2257–2271.
- Hajibabdolmajid V. R., 2001. Mobilization of strength in brittle failure of rock, Ph.D. thesis, Department of Mining Engineering, Queen's University, Kingston, Canada.
- Hoek, E., Brown, E., 1980. Empirical strength criterion for rock masses. Journal of the Geotechnical Engineering Division 106 (GT9), 1013–1035.
- Hudson, J.A., Harrison, J.P., 1997. Engineering Rock Mechanics: An Introduction to the Principles. Pergamon.
- Li, Xiaochun, Xu, Dongjun, 1991. Law and degree of effect the intermediate principle stress on strength of rock. Rock and Soil Mechanics 12 (1), 10–16.
- Liu, Dongjun, Cao, Jie, 2008. Test and study of influence of intermediate main stress to characteristic of rock mechanics. Yellow River 30 (1), 59–61.
- Martin, C.D., 1997. Seventeenth Canadian geotechnical colloquium: the effect of cohesion loss and stress path on brittle rock strength. Canadian Geotechnical Journal 34 (5), 698–725.
- Mogi, K., 1979. Flow and Fracture of Rocks under General Triaxial Compression. Proceedings of the Fourth Congress ISRM, vol. 3. Rotterdam, Balkema, pp. 123–130.
- Mogi, K., 2007. Experimental Rock Mechanics. Taylor & Francis/Balkema, London.
- Owen, D.R.J., Hinton, E., 1980. Finite Element in Plasticity: Theory and Practice. Pinerige Press Ltd.
- Pan, P.Z., Feng, X.T., Hudson, J.A., 2006. Numerical simulations of Class I and Class II uniaxial compression curves using an elasto-plastic cellular automaton and a linear combination of stress and strain as the control method. International Journal of Rock Mechanics & Mining Sciences 43 (7), 1109–1117.
- Pan, P.Z., Feng, X.T., Hudson, J.A., 2009. Study of failure and scale effects in rocks under uniaxial compression using 3D cellular automata. International Journal of Rock Mechanics & Mining Sciences 46 (4), 674–685.
- Shi, Lu, Li, Xiaochun, 2009. Analysis of end friction effect in true triaxial test. Rock and Soil Mechanics 30 (4), 1159–1164.
- Tang, C.A., Hudson, J.A., 2010. Rock Failure Mechanisms: Explained and Illustrated. Taylor and Francis, London.
- Weibull, W., 1951. A statistical distribution function of wide applicability. Journal of Applied Mechanics 18 (3), 293–297.
- Wiebols, G.A., Cook, N.G.W., 1968. An energy criterion for the strength of rock in polyaxial compression. International Journal of Rock Mechanics & Mining Sciences 5, 529–549.
- Xu, Dongjun, Geng, Naiguang, 1985. The variation law of rock strength with increase of intermediate principal stress. Acta Mechanica Solida Sinica 1, 72–80.
- Xu, Dongjun, Geng, Naiguang, 1989. The effect of intermediate principal stress on the load bearing capacity of fractured rock. Acta Geophysics Sinica 32 (Suppl. 1), 253–259.
- Yang, Jihua, Liu, Handong, 2007. True triaxial experimental study on rock strength and deformation. Journal of North China Institute of Water Conservancy and Hydroelectric Power 28 (3), 66–68.
- Zhou, A., 1994. A program to model the initial shape and extent of borehole breakout. Computers and Geosciences 20 (7/8), 1143–1160.